Homogeneous Catalytic Reduction of O_2 to H_2O by a Terpyridine-Based FeN_3O Complex

Emma N. Cook,[#] Shelby L. Hooe,[#] Diane A. Dickie, and Charles W. Machan*

Department of Chemistry, University of Virginia,
PO Box 400319, Charlottesville, VA 22904-4319

[#] - *equal author contribution*

* - machan@virginia.edu; ORCID 0000-0002-5182-1138

E.N.C. ORCID 0000-0002-0568-3600; S.L.H. ORCID 0000-0002-6991-2273; D.A.D. ORCID 0000-0003-0939-3309

Abstract

We report a new terpyridine-based FeN_3O catalyst, $Fe(tpy^{tbu}pho)Cl_2$, which reduces O_2 to H_2O. Variable concentration and variable temperature spectrochemical studies with decamethylferrocene as a chemical reductant in acetonitrile solution enabled the elucidation of key reaction parameters for the catalytic reduction of O_2 to H_2O by $Fe(tpy^{tbu}pho)Cl_2$. These mechanistic studies suggest that a 2+2 mechanism is operative, where hydrogen peroxide is produced as a discrete intermediate, prior to further reduction to H_2O. Consistent with this proposal, the spectrochemically measured k_{cat} values for H_2O_2 reduction is larger than that for O_2 reduction. Further, significant H_2O_2 production is observed under hydrodynamic conditions in rotating ring-disk electrode measurements, where the product can be swept away from the cathode surface before further reduction occurs.

Introduction

In response to rising concerns over increasing energy demands and anthropogenic CO_2 emissions, the catalytic reduction of dioxygen to water remains a reaction of interest for the development of next-generation fuel cell technologies.[1-4] Of the earth abundant molecular catalysts for O_2 reduction,[2] Fe porphyrin- and phthalocyanine-based complexes remain among the most studied and robust catalysts.[5-12] It is conspicuous that non-heme systems are understudied relative to these examples, given the abundance of enzymes which contain a non-heme Fe center capable of reactivity with O_2 in order to carry out a variety of biologically relevant reactions.[13-18] In spite of this, molecular non-heme Fe catalysts capable of the O_2 reduction reaction (ORR) are exceedingly rare.[19-21]

Previous O_2 reduction studies from our lab identified non-heme molecular Mn[22-24] and Co[25-26] catalyst systems based on a bpy-based dianionic N_2O_2 ligand framework (bpy = 2,2-bipyridine), as well as an Fe complex in a non-conjugated $[N_3O]^-$ donor framework inspired by mononuclear non-heme metallocofactors.[21] Motivated by the scarcity of non-heme Fe catalysts for ORR[20-21, 27] and reasoning that conjugated polypyridine frameworks could be beneficial for similar reasons that they are useful in electrocatalytic carbon dioxide reduction,[28] we have identified a new Fe complex for the ORR using a conjugated tpy-based monoanionic $[N_3O]^-$ ligand framework. Herein, we present a new molecular Fe catalyst, Fe(tpy^{tbu}pho)Cl_2, where 2-([2,2':6',2''-terpyridin]-6-yl)-4,6-di-*tert*-butylphenolate = [tpy^{tbu}pho]$^-$, which is active for electrochemical O_2 reduction to H_2O. Mechanistic analysis using spectrochemical stopped-flow methods with decamethylferrocene (Cp^*_2Fe) as a homogeneous reductant in acetonitrile (MeCN) solution shows ORR is limited by O_2

binding to the singly reduced metal center and where H_2O_2 is implicated as a discrete intermediate prior to further reduction to H_2O.

Results

The synthesis of 2-([2,2':6',2''-terpyridin]-6-yl)-4,6-di-tert-butylphenol, tpy^{tbu}pho(H), was carried out via a modified literature procedure using Pd-catalyzed cross-coupling.[22, 29] The Fe(tpy^{tbu}pho)Cl_2 complex was synthesized by sequentially combining the purified ligand with sodium acetate in ethanol solution followed by Fe(III) chloride hexahydrate, prior to isolation and recrystallization (See **Materials and Methods** Section of SI for detailed procedures).[30] Fe(tpy^{tbu}pho)Cl_2 was characterized via ESI-MS, EA, NMR, and UV-vis spectroscopies (SI **Materials and Methods** Section, **Table S1**, and **Figures S1-S2**). The proposed molecular connectivity was supported by structural data obtained from single-crystal X-ray diffraction studies (**Figure 1**).

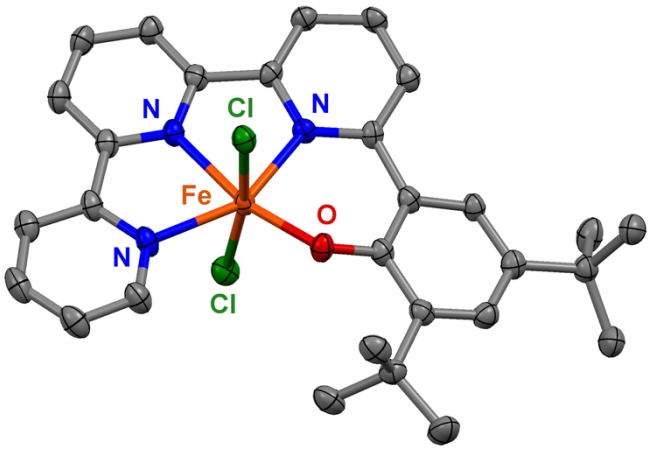

Figure 1. Molecular structure of Fe(tpy^{tbu}pho)Cl_2 obtained from single-crystal X-ray diffraction studies. Blue = N, red = O, gray = C, green = Cl, orange = Fe; thermal ellipsoids at 50%; hydrogen atoms and non-coordinating solvent omitted for clarity; CCDC 2097186.

Cyclic voltammetry (CV) experiments were performed on Fe(tpy^{tbu}pho)Cl_2 in a solution of 0.1 M tetrabutylammonium hexafluorophosphate ($TBAPF_6$) in MeCN. Under argon (Ar)

saturation conditions, Fe(tpy^{tbu}pho)Cl_2 displays a single redox feature at $E_{1/2}$ = –0.51 V vs Fc^+/Fc (**Figure 2**, black). This reversible feature is attributed to a formal $Fe^{III/II}$ reduction, given its general agreement with related Fe(III) compounds.[30-31] Under O_2 saturation conditions, this redox feature becomes irreversible with E_p = –0.65 V vs Fc^+/Fc (**Figure 2**, red), suggesting O_2 binding to a formally Fe(II) metal center. Variable scan rate studies at low scan rates under Ar saturation indicated that delayed chloride loss did not cause the observed loss of reversibility (**Figure S3**). Under Ar saturation conditions, there is an observed potential dependence on the presence of acetic acid (AcOH), where addition of 0.0875 M AcOH results in a positive shift of 0.15 V in the $Fe^{III/II}$ redox to an $E_{1/2}$ = –0.36 V vs Fc^+/Fc (**Figure 2**, green). This potential shift exhibited a concentration dependence suggestive of an equilibrium reaction: increasing the concentration of AcOH to 0.35 M resulted in a shift to $E_{1/2}$ = –0.25 V (**Figure S4**).

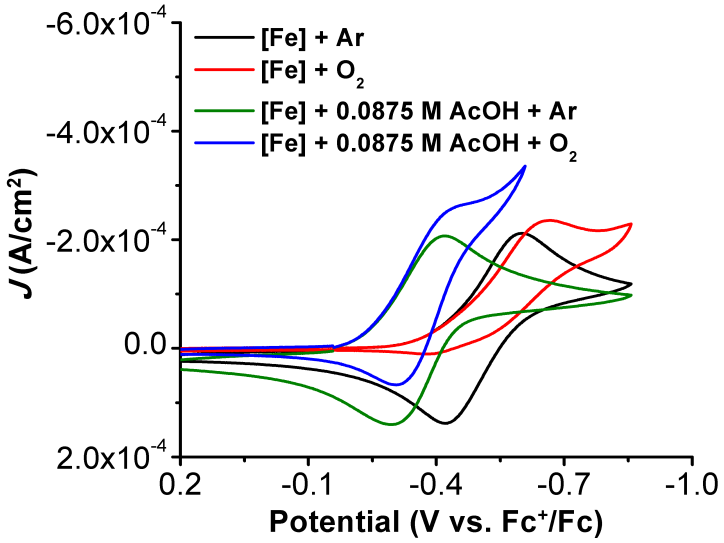

Figure 2. Comparison of CVs of Fe(tpy^{tbu}pho)Cl_2 under Ar and O_2 saturation conditions with and without 0.0875 M AcOH. Conditions: 1.0 mM Fe(tpy^{tbu}pho)Cl_2 in 0.1 M $TBAPF_6$/MeCN; glassy carbon working electrode, glassy carbon rod counter electrode, Ag/AgCl pseudoreference electrode; referenced to Fc^+/Fc internal standard; 100 mV/s scan rate.

To understand the nature of chloride ligand solvation under these conditions, we conducted an AcOH titration under an inert atmosphere (Ar) with Fe(tpy^{tbu}pho)Cl_2 in the presence of tetrabutylammonium chloride (TBACl) as a Cl^- donor (**Figure S5**). With excess Cl^- present, a negative potential shift of the $Fe^{III/II}$ feature to $E_{1/2}$ = –0.64 V vs Fc^+/Fc is observed for Fe(tpy^{tbu}pho)Cl_2, consistent with the inhibition of a pre-equilibrium displacement of an axial Cl^- ligands by MeCN. Titrating increasing amounts of AcOH up to 0.63 M in the presence of 0.1 M TBACl lead to a loss of reversibility at $E_{1/2}$ = –0.64 V vs Fc^+/Fc and the appearance of a new reversible feature at $E_{1/2}$ = –0.40 V vs Fc^+/Fc. Based on these data, it is proposed that the observed shifts to positive potentials when AcOH is introduced into solution originates from the favorable solvation of the Cl^- counteranions, assisted by MeCN coordination to Fe. Therefore, the following assignments for the standard reduction potentials of the following chloro and solvento species can be made, where *L* = [tpy^{tbu}pho]$^-$. Note that **Eq (1)** and **Eq (2)** were assigned based on the data described above obtained with added TBACl and AcOH (**Figure S5**) while **Eq (3)** was determined from experiments with added AcOH only (**Figure S4**).

$$[Fe(L)Cl_2] + e^- \rightleftharpoons [Fe(L)Cl_2]^- \qquad E^0 = -0.64\ V\ vs\ Fc^+/Fc \qquad \textbf{Eq (1)}$$

$$[Fe(L)Cl(MeCN)]^+ + e^- \rightleftharpoons [Fe(L)Cl(MeCN)]^+ \qquad E^0 = -0.40\ V\ vs\ Fc^+/Fc \qquad \textbf{Eq (2)}$$

$$[Fe(L)(MeCN)_2]^{2+} + e^- \rightleftharpoons [[Fe(L)(MeCN)_2]^+ \qquad E^0 = -0.25\ V\ vs\ Fc^+/Fc \qquad \textbf{Eq (3)}$$

Under O_2 saturation conditions with 0.0875 M AcOH there is an increase in current at the $Fe^{III/II}$ redox event, suggesting catalytic activity toward the ORR under electrochemical conditions (**Figure 2**, blue). Rotating ring-disk electrode methods were used to determine the selectivity of the ORR under electrochemical conditions, revealing a H_2O_2 selectivity of 70.0 ± 8.6%. At rotation rates greater than 1800 rpm, H_2O_2 is the exclusive product, suggesting that H_2O_2 is produced as a discrete intermediate, *vide infra* (See **SI**).

Because minimal catalytic current increase precluded us from further mechanistic analysis under electrochemical conditions, mechanistic studies were conducted using decamethylferrocene (Cp^*_2Fe) as a chemical reductant. In MeCN with 0.35 M AcOH present the $Fe^{III/II}$ reduction potential of $Fe(tpy^{tbu}pho)Cl_2$ ($E_{1/2}$ = –0.25 V vs Fc^+/Fc, **Figure S3**) is sufficiently positive of Cp^*_2Fe ($E_{1/2}$ = –0.51 V vs Fc^+/Fc[32]) for favorable electron transfer, with an equilibrium constant (K_{ET}) of 2.5 x 10^4 (See **SI**). We note that although there is a dependence of the $Fe^{III/II}$ redox potentials on AcOH concentration, $E_{1/2}$ values observed at lower AcOH concentrations are still sufficiently positive ($E_{1/2}$ = –0.36 V vs Fc^+/Fc with 0.0875 M AcOH) for favorable electron transfer from Cp^*_2Fe, even as [AcOH] decreases over the course of the catalytic reaction. Rapid-mixing UV-vis stopped-flow experiments revealed that the ORR mediated by $Fe(tpy^{tbu}pho)Cl_2$ exhibits a first-order dependence on the [O_2] and [Cp^*_2Fe] (**Figure 3A** and **3B**, respectively). No dependence on [AcOH] was observed, suggesting saturation of the catalytic response at low acid concentrations (**Figure 3C**). Interestingly, when the concentration of $Fe(tpy^{tbu}pho)Cl_2$ was varied, two distinct regions were observed (**Figure 3D**). At low [Fe] (<12.6 μM), a first-order dependence is observed before the effect of increasing [Fe] on the apparent rate begins to saturate, and a plateau region is observed. Control studies showed negligible background reactivity without the presence of $Fe(tpy^{tbu}pho)Cl_2$ (**Figure S9**). Based on these mechanistic studies, we can propose the following rate expression for the ORR, **Eq (4)**:

$$rate = k_{cat}[Fe]^1[acid]^0[O_2]^1[Cp^*_2Fc]^1 \quad \textbf{Eq (4)}$$

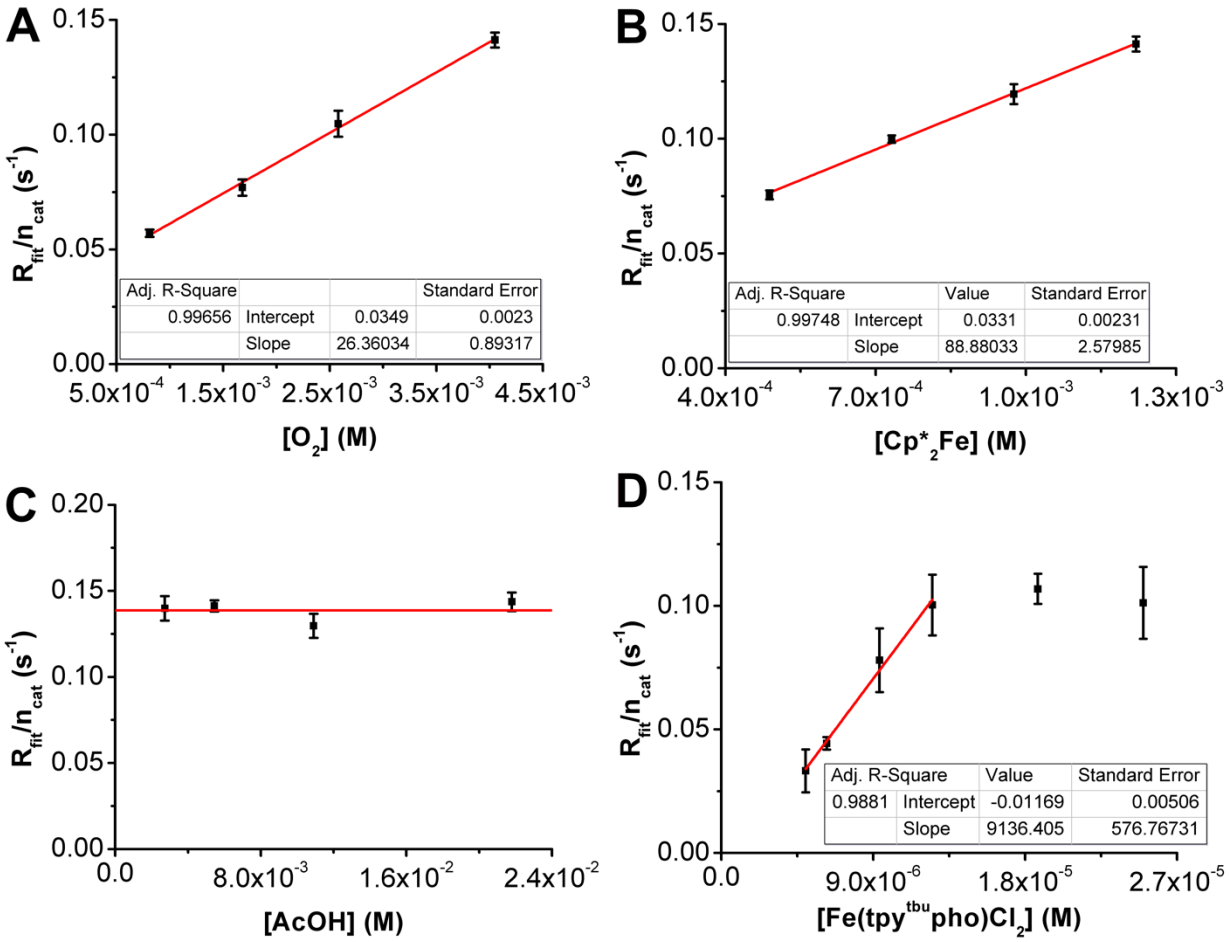

Figure 3. The calculated R_{fit}/n_{cat} from stopped-flow spectrochemical experiments where the concentration of O_2 (**A**), Cp^*_2Fe (**B**), AcOH (**C**), and $Fe(tpy^{tbu}pho)Cl_2$ (**D**), and were each independently varied at 25.5°C in MeCN. The horizontal line in (**C**) represents the global average rate observed across all experiments for variable [AcOH]. Data were fit using Kinetic Studio 4.0 (2 Exp + Mx + C). See Material and Methods section for syringe concentrations used.

With a fixed concentration ratio, analogous experiments were repeated at variable temperatures, enabling Eyring analysis to determine the reaction parameters of the rate-determining step (**Figure S10 and Table S2**). These lead to an estimated barrier $\Delta G^{\ddagger}_{298K}$ of +10.1 kcal/mol, **Eqs (5)** and **(6)**.

$$\Delta G^{\ddagger} = \Delta H^{\ddagger} - T\Delta S^{\ddagger} \qquad \textbf{Eq (5)}$$

$$\Delta G^{\ddagger} = 3.72\,\frac{kcal}{mol} - T\left(-21.4\,\frac{cal}{mol \cdot K}\right) \qquad \textbf{Eq (6)}$$

The product selectivity of ORR mediated by Fe(tpy^{tbu}pho)Cl_2 was determined by spectrophotometric methods to be quantitative for H_2O, with no detectable amount of H_2O_2 (**Figure S11**). UV-vis studies carried out with Fe(tpy^{tbu}pho)Cl_2 and urea•H_2O_2 eliminate disproportionation of H_2O_2 by Fe(tpy^{tbu}pho)Cl_2 as a possible mechanistic pathway (**Figure S12**). These data showed that H_2O_2 is stable in the presence of Fe(tpy^{tbu}pho)Cl_2 without added Cp^*_2Fe (**Figures S12-S13**). However, with added chemical reductant in solution, the system catalytically reduces H_2O_2 to water via a $2H^+/2e^-$ pathway, implicating a 2+2 mechanism for the observed ORR. Control studies showed negligible reactivity for H_2O_2 reduction without the presence of Fe(tpy^{tbu}pho)Cl_2 (**Figure S14**). Further, reaction stoichiometry of hydrogen peroxide reduction (H_2O_2RR) by Fe(tpy^{tbu}pho)Cl_2 was found to be 2.09 ± 0.1 (**Figure S15**, see **SI**).

An average third-order rate constant ($k_{cat,ORR}$) for O_2 reduction to H_2O by Fe(tpy^{tbu}pho)Cl_2 was subsequently derived (n_{cat} = 4), based on the previously derived catalytic rate expression **Eq (7)** (see **SI**).

$$\frac{R_{fit}}{n_{cat}} = k_{cat}[catalyst]^1[O_2]^1[Cp^*_2Fc]^1 \qquad \textbf{Eq (7)}$$

$k_{cat,ORR}$ = 1.13 ± 0.62 x 10^9 M^{-2} s^{-1}

Based on the observed activity for H_2O_2RR (**Figure S14**), mechanistic studies were again conducted using UV-vis stopped-flow spectroscopy. Variable concentration studies under anaerobic conditions revealed a rate law of H_2O_2RR by Fe(tpy^{tbu}pho)Cl_2 that is first order with respect to [catalyst] and [H_2O_2], but zero order with respect to [Cp_2*Fe] and [AcOH] (**Eq (8)**, **Figures S16-S19**) with an average second-order catalytic rate constant $k_{cat,H2O2RR}$ of 1.02 ± 0.10 x 10^7 M^{-1} s^{-1} using **Eq (8)** (see **SI**).

$$\frac{R_{fit}}{n_{cat}} = k_{cat}[catalyst]^1[H_2O_2]^1 \qquad \textbf{Eq (8)}$$

$k_{cat,H2O2RR}$ = 1.02 ± 0.20 x 10^7 M^{-1} s^{-1}

Determination of effective overpotentials (η) for ORR and H_2O_2RR in this system is complicated due to the lack of catalytic activity under buffered conditions (**Figure S20**). However, we are able to generate approximate η values using corrected standard reduction potentials that account for pK_a (23.5) and log(K_{AHA}) of AcOH in MeCN (see SI), where η_{ORR} = 0.24 V and η_{H2O2RR} = 0.83 V.[33-35] We emphasize that these values should be considered a *lower-limit approximation* of the true thermodynamic potential since buffered conditions could not be directly assessed.

In order to better understand the mechanism of ORR mediated by Fe(tpy^{tbu}pho)Cl_2, we synthesized both [Fe(tpy^{tbu}pho)][OTf]$_2$ and a model of the Fe(II) intermediate [Fe^{II}(tpy^{tbu}pho)][OTf], where OTf is the non-coordinating anion trifluoromethanesulfonate. CVs of [Fe(tpy^{tbu}pho)][OTf]$_2$ obtained under Ar saturation show a small irreversible reduction wave at E_p = –0.26 V vs. Fc^+/Fc, followed by an irreversible reduction wave at E_p =–0.80 V vs. Fc^+/Fc, the latter of which is attributed to the $Fe^{III/II}$. Upon the addition of 0.35 M AcOH, the $Fe^{III/II}$ feature becomes reversible and shifts to $E_{1/2}$ = –0.32 V vs. Fc^+/Fc, consistent with the $E_{1/2}$ = –0.25 V observed for Fe(tpy^{tbu}pho)Cl_2 under comparable conditions (**Figure S22**). Additionally, UV-vis spectroscopic studies of both Fe(tpy^{tbu}pho)Cl_2 and [Fe(tpy^{tbu}pho)][OTf]$_2$ show similar spectral changes upon addition of increasing amounts of AcOH, supporting the proposal that both complexes form similar solvent species under protic conditions (**Figure S24**).

Discussion

From these data, we are able to propose a 2+2 catalytic cycle for the ORR by Fe(tpy^{tbu}pho)Cl_2 (**Scheme 1**). Based on electrochemical data (Figure S5), AcOH facilitates the loss of two Cl^- anions with MeCN coordination to form $[Fe(tpy^{tbu}pho)(MeCN)_2]^{2+}$ (**2**) which undergoes a favorable one-electron reduction process (K_{ET} = 2.5 x 10^4, see SI) to form an Fe(II) species, **3**, that is the resting state of the catalyst. Rate-limiting O_2 binding is proposed to form an unobserved Fe(III) superoxide intermediate **4**. Consistent with this interpretation, mechanistic UV-vis and ^{1}H-NMR spectroscopic studies with a chemically prepared model of the active catalyst, $[Fe^{II}(tpy^{tbu}pho)][OTf]$, showed slow conversion following O_2 exposure, with Fe^{II} fully consumed after 18 h (**Figures S25-S28**).

Subsequently **4** undergoes net reduction and protonation to regenerate **2** and an equivalent of H_2O_2. As described above, control testing showed no interaction between H_2O_2 and the pre-catalytic Fe(III) state. The proposal of H_2O_2 as a discrete intermediate is directly supported by the observation of 70.0 ± 8.6% selectivity for H_2O_2 during RRDE experiments and quantitative selectivity for H_2O under spectrochemical conditions because of the difference in timescale of each experiment. During RRDE, H_2O_2 produced during the ORR, as well as any unreacted Fe(II) species, are rapidly swept away from the disk electrode for oxidation at the Pt ring electrode (~1 s). However, in the Ti(O)SO_4 titration experiment used for spectrochemical quantification, the catalytic solution that contains catalyst, reductant, O_2, and a proton source is not analyzed until the completion of the reaction (~5 min), such that any H_2O_2 produced during catalysis is further reduced to H_2O.

Since H_2O is observed to be the final product under spectrochemical conditions, we propose that **2** undergoes rapid reduction and H_2O_2 binding followed by additional reduction and protonation reactions to generate two equivalents of H_2O and reform **2**, based on the observed rate law of the ORR and H_2O_2RR by Fe(tpy^{tbu}pho)Cl_2. Comparable first-order rate constants k (s^{-1}) for ORR and H_2O_2RR are represented by the slopes of the variable O_2 (**Figure 2A**) and variable H_2O_2 (**Figure S15**) data: k for H_2O_2RR (178 s^{-1}) is more than 6-fold greater than for ORR (26.4 s^{-1}). The difference in first-order rate constants is consistent with the intermediate reaction selectivity observed during RRDE experiments below 1800 rpm, as well as the shift to quantitative H_2O_2 production at higher rotation rates.

Scheme 1. Proposed Catalytic Cycle for ORR Mediated by Fe(tpy^{tbu}pho)Cl_2.

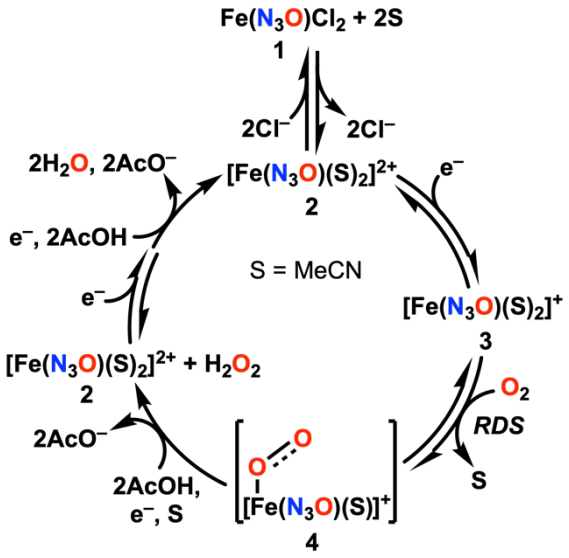

Recently, we reported 2+2 ORR activity by an Fe complex with a bioinspired $[N_3O]^-$ ligand framework, *N*,*N*′-bis(2-pyridylmethyl)glycinate or PMG.[21] Mechanistically, one of the defining features of the ORR mediated by Fe(PMG)Cl_2 is an off-cycle peroxo dimer, which was observed to be the resting state of the catalytic cycle. The 2+2 cycle itself also

showed a greater disparity between the rates of the two reactions than is observed here for Fe(tpy^{tbu}pho)Cl_2: the observed TOF for ORR mediated by Fe(PMG)Cl_2 was 0.92 s^{-1} and that for H_2O_2RR was 2.9 x 10^3 s^{-1}, a ~3200-fold difference. Although in-depth mechanistic comparisons between the two complexes are beyond the scope of the present study, it is worth noting some of the key differences between the two in the context of their reactivity. Although when both complexes are reduced to the Fe(II) state a favorable reaction with O_2 occurs, the resulting superoxo species are likely to be quite different. For the Fe(tpy^{tbu}pho)Cl_2 system, an MeCN solvent molecule will be opposite the site of O_2 binding, whereas in Fe(PMG)Cl_2 a more basic trialkylamine fragment from the ligand framework will occupy this position. Axial ligand effects on peroxo dimerization and O–O bond scission are well-known and previously reported trends are consistent with the increased H_2O_2RR TOF for Fe(PMG)Cl_2 and its greater axial ligand basicity in comparison to Fe(tpy^{tbu}pho)Cl_2.[2, 36-37]

Conclusion

Non-heme iron electrocatalysts for the ORR have been relatively under-studied in comparison to porphyrin-based systems. Here, we have reported a novel non-heme Fe complex containing an N_3O terpyridine-based ligand framework (Fe(tpy^{tbu}pho)Cl_2) that is electrocatalytically active toward the reduction of O_2 to H_2O where H_2O_2 is produced as a discrete intermediate during catalysis. Mechanistic analysis revealed that the rate of ORR is limited by O_2 binding to the Fe(II) metal center. Additionally, it is implied that ORR by Fe(tpy^{tbu}pho)Cl_2 proceeds via 2+2 mechanism, where H_2O_2 produced during catalysis is further reduced by $2H^+/2e^-$ to two equivalents of H_2O. Ligand modification to tune ORR reactivity and selectivity is a focus of ongoing work.

Associated Content

Supporting information

Supporting Information can be found at XXX. SI includes synthetic summaries, NMR and UV-vis characterization, electrochemistry, and description of experimental details and methods, as well as a separate file containing computational coordinates.

Accession Codes

CCDC 2097186-2097187 contains the supplementary crystallographic data for this paper. These data can be obtained free of charge via www.ccdc.cam.ac.uk/data_request/cif, or by emailing data_request@ccdc.cam.ac.uk, or by contacting The Cambridge Crystallographic Data Centre, 12 Union Road, Cambridge CB2 1EZ, UK; fax: +44 1223 336033.

Author Information

Corresponding Author

Charles W. Machan – Department of Chemistry, University of Virginia, Charlottesville, Virginia 22904-4319, United States; orcid.org/0000-0002-5182-1138;

Email: machan@virginia.edu

Authors:

Emma N. Cook – Department of Chemistry, University of Virginia, Charlottesville, Virginia 22904-4319, United States; orcid.org/0000-0002-0568-3600

Shelby L. Hooe – Department of Chemistry, University of Virginia, Charlottesville, Virginia 22904-4319, United States; orcid.org/0000-0002-6991-2273

Diane A. Dickie – Department of Chemistry, University of Virginia, Charlottesville, Virginia 22904-4319, United States; orcid.org/0000-0003-0939-3309

Author Contributions

The manuscript was written through the contribution of all authors. We thank Dr. Juan J. Moreno for initial contributions to the project.

Funding Sources

We thank the University of Virginia for infrastructural support. E.N.C, S.L.H., and C.W.M. acknowledge N.S.F. CHE-2102156 and ACS PRF 61430-ND3 for support. Single crystal X-ray diffraction experiments were performed on a diffractometer at the University of Virginia funded by the NSF-MRI program (CHE-2018870).

References

1. Sahu, S.; Goldberg, D. P., Activation of Dioxygen by Iron and Manganese Complexes: A Heme and Nonheme Perspective. *J. Am. Chem. Soc.* **2016,** *138* (36), 11410-28.
2. Pegis, M. L.; Wise, C. F.; Martin, D. J.; Mayer, J. M., Oxygen Reduction by Homogeneous Molecular Catalysts and Electrocatalysts. *Chem. Rev.* **2018,** *118* (5), 2340-2391.
3. IPCC *Global Warming of 1.5°C. An IPCC Special Report*; World Meterological Organization: Geneva, Switzerland, 2018.
4. Machan, C. W., Advances in the Molecular Catalysis of Dioxygen Reduction. *ACS Catal.* **2020,** *10* (4), 2640-2655.
5. Martin, D. J.; Wise, C. F.; Pegis, M. L.; Mayer, J. M., Developing Scaling Relationships for Molecular Electrocatalysis through Studies of Fe-Porphyrin-Catalyzed O2 Reduction. *Acc. Chem. Res.* **2020,** *53* (5), 1056-1065.
6. Pegis, M. L.; Martin, D. J.; Wise, C. F.; Brezny, A. C.; Johnson, S. I.; Johnson, L. E.; Kumar, N.; Raugei, S.; Mayer, J. M., Mechanism of Catalytic O2 Reduction by Iron Tetraphenylporphyrin. *J. Am. Chem. Soc.* **2019,** *141* (20), 8315-8326.
7. Pegis, M. L.; McKeown, B. A.; Kumar, N.; Lang, K.; Wasylenko, D. J.; Zhang, X. P.; Raugei, S.; Mayer, J. M., Homogenous Electrocatalytic Oxygen Reduction Rates Correlate with Reaction Overpotential in Acidic Organic Solutions. *ACS Cent. Sci.* **2016,** *2* (11), 850-856.
8. Pegis, M. L.; Wise, C. F.; Koronkiewicz, B.; Mayer, J. M., Identifying and Breaking Scaling Relations in Molecular Catalysis of Electrochemical Reactions. *J. Am. Chem. Soc.* **2017,** *139* (32), 11000-11003.
9. Wasylenko, D. J.; Rodríguez, C.; Pegis, M. L.; Mayer, J. M., Direct Comparison of Electrochemical and Spectrochemical Kinetics for Catalytic Oxygen Reduction. *J. Am. Chem. Soc.* **2014,** *136* (36), 12544-12547.
10. Wang, Y.-H.; Pegis, M. L.; Mayer, J. M.; Stahl, S. S., Molecular Cobalt Catalysts for O2 Reduction: Low-Overpotential Production of H2O2 and Comparison with Iron-Based Catalysts. *J. Am. Chem. Soc.* **2017,** *139* (46), 16458-16461.

11. Brezny, A. C.; Johnson, S. I.; Raugei, S.; Mayer, J. M., Selectivity-Determining Steps in O2 Reduction Catalyzed by Iron(tetramesitylporphyrin). *J. Am. Chem. Soc.* **2020,** *142* (9), 4108-4113.
12. Kobayashi, N.; Nevin, W. A., Electrocatalytic Reduction of Oxygen Using Water-Soluble Iron and Cobalt Phthalocyanines and Porphyrins. *Appl. Organomet. Chem.* **1996,** *10* (8), 579-590.
13. Yang, Y.-S.; Baldwin, J.; Ley, B. A.; Bollinger, J. M.; Solomon, E. I., Spectroscopic and Electronic Structure Description of the Reduced Binuclear Non-Heme Iron Active Site in Ribonucleotide Reductase from E. coli: Comparison to Reduced Δ9 Desaturase and Electronic Structure Contributions to Differences in O2 Reactivity. *J. Am. Chem. Soc.* **2000,** *122* (35), 8495-8510.
14. Wang, Y.; Li, J.; Liu, A., Oxygen activation by mononuclear nonheme iron dioxygenases involved in the degradation of aromatics. *JBIC J. Biol. Inorg. Chem.* **2017,** *22* (2), 395-405.
15. Bassan, A.; Blomberg, M. R. A.; Borowski, T.; Siegbahn, P. E. M., Oxygen Activation by Rieske Non-Heme Iron Oxygenases, a Theoretical Insight. *J. Phys. Chem. B* **2004,** *108* (34), 13031-13041.
16. Brown, K. A.; Guo, Z.; Tokmina-Lukaszewska, M.; Scott, L. W.; Lubner, C. E.; Smolinski, S.; Mulder, D. W.; Bothner, B.; King, P. W., The oxygen reduction reaction catalyzed by Synechocystis sp. PCC 6803 flavodiiron proteins. *Sustain. Energy & Fuels* **2019,** *3* (11), 3191-3200.
17. Solomon, E. I.; Decker, A.; Lehnert, N., Non-heme iron enzymes: Contrasts to heme catalysis. *Proc. Natl. Acad. Sci. USA* **2003,** *100* (7), 3589-3594.
18. Abu-Omar, M. M.; Loaiza, A.; Hontzeas, N., Reaction Mechanisms of Mononuclear Non-Heme Iron Oxygenases. *Chem. Rev.* **2005,** *105* (6), 2227-2252.
19. Lu, X.; Lee, Y.-M.; Sankaralingam, M.; Fukuzumi, S.; Nam, W., Catalytic Four-Electron Reduction of Dioxygen by Ferrocene Derivatives with a Nonheme Iron(III) TAML Complex. *Inorg. Chem.* **2020,** *59* (24), 18010-18017.
20. Wang, L.; Gennari, M.; Cantú Reinhard, F. G.; Gutiérrez, J.; Morozan, A.; Philouze, C.; Demeshko, S.; Artero, V.; Meyer, F.; de Visser, S. P.; Duboc, C., A Non-Heme Diiron Complex for (Electro)catalytic Reduction of Dioxygen: Tuning the Selectivity through Electron Delivery. *J. Am. Chem. Soc.* **2019,** *141* (20), 8244-8253.
21. Cook, E. N.; Dickie, D. A.; Machan, C. W., Catalytic Reduction of Dioxygen to Water by a Bioinspired Non-Heme Iron Complex via a 2+2 Mechanism. *J. Am. Chem. Soc.* **2021,** *143* (40), 16411-16418.
22. Hooe, S. L.; Rheingold, A. L.; Machan, C. W., Electrocatalytic Reduction of Dioxygen to Hydrogen Peroxide by a Molecular Manganese Complex with a Bipyridine-Containing Schiff Base Ligand. *J. Am. Chem. Soc.* **2018,** *140* (9), 3232-3241.
23. Hooe, S. L.; Machan, C. W., Dioxygen Reduction to Hydrogen Peroxide by a Molecular Mn Complex: Mechanistic Divergence between Homogeneous and Heterogeneous Reductants. *J. Am. Chem. Soc.* **2019,** *141* (10), 4379-4387.
24. Hooe, S. L.; Cook, E. N.; Reid, A. G.; Machan, C. W., Non-covalent assembly of proton donors and p-benzoquinone anions for co-electrocatalytic reduction of dioxygen. *Chem. Sci.* **2021,** *12* (28), 9733-9741.

25. Nichols, A. W.; Kuehner, J. S.; Huffman, B. L.; Miedaner, P. R.; Dickie, D. A.; Machan, C. W., Reduction of dioxygen to water by a Co(N2O2) complex with a 2,2′-bipyridine backbone. *Chem. Commun.* **2021,** *57* (4), 516-519.
26. Nichols, A. W.; Cook, E. N.; Gan, Y. J.; Miedaner, P. R.; Dressel, J. M.; Dickie, D. A.; Shafaat, H. S.; Machan, C. W., Pendent Relay Enhances H2O2 Selectivity during Dioxygen Reduction Mediated by Bipyridine-Based Co–N2O2 Complexes. *J. Am. Chem. Soc.* **2021,** *143* (33), 13065-13073.
27. Gordon, J. B.; Vilbert, A. C.; Dimucci, I. M.; MacMillan, S. N.; Lancaster, K. M.; Moënne-Loccoz, P.; Goldberg, D. P., Activation of Dioxygen by a Mononuclear Nonheme Iron Complex: Sequential Peroxo, Oxo, and Hydroxo Intermediates. *J. Am. Chem. Soc.* **2019,** *141* (44), 17533-17547.
28. Elgrishi, N.; Chambers, M. B.; Wang, X.; Fontecave, M., Molecular polypyridine-based metal complexes as catalysts for the reduction of CO2. *Chem. Soc. Rev.* **2017,** *46* (3), 761-796.
29. Hooe, S. L.; Moreno, J. J.; Reid, A. G.; Dickie, D. A.; Machan, C. W., Homogeneous Electrocatalytic Reduction of CO2 by a CrN3O Complex: Electronic Coupling with Redox-Active Terpyridine Fragment Favors Selectivity for CO. *ChemRxiv* **2021**, 10.33774/chemrxiv-2021-lplvt.
30. Nichols, A. W.; Chatterjee, S.; Sabat, M.; Machan, C. W., Electrocatalytic Reduction of CO2 to Formate by an Iron Schiff Base Complex. *Inorg. Chem.* **2018,** *57* (4), 2111-2121.
31. Nichols, A. W.; Hooe, S. L.; Kuehner, J. S.; Dickie, D. A.; Machan, C. W., Electrocatalytic CO2 Reduction to Formate with Molecular Fe(III) Complexes Containing Pendent Proton Relays. *Inorg. Chem.* **2020,** *59* (9), 5854-5864.
32. Noviandri, I.; Brown, K. N.; Fleming, D. S.; Gulyas, P. T.; Lay, P. A.; Masters, A. F.; Phillips, L., The Decamethylferrocenium/Decamethylferrocene Redox Couple: A Superior Redox Standard to the Ferrocenium/Ferrocene Redox Couple for Studying Solvent Effects on the Thermodynamics of Electron Transfer. *J. Phys. Chem. B* **1999,** *103* (32), 6713-6722.
33. McCarthy, B. D.; Martin, D. J.; Rountree, E. S.; Ullman, A. C.; Dempsey, J. L., Electrochemical Reduction of Brønsted Acids by Glassy Carbon in Acetonitrile—Implications for Electrocatalytic Hydrogen Evolution. *Inorg. Chem.* **2014,** *53* (16), 8350-8361.
34. Matsubara, Y., Unified Benchmarking of Electrocatalysts in Noninnocent Second Coordination Spheres for CO2 Reduction. *ACS Energy Lett.* **2019,** *4* (8), 1999-2004.
35. (a) Costentin, C., Molecular Catalysis of Electrochemical Reactions. Overpotential and Turnover Frequency: Unidirectional and Bidirectional Systems. *ACS Catalysis* **2021,** *11* (9), 5678-5687. (b) Note that effective overpotentials for chemical reactions with homogeneous reductants cannot be directly compared to overpotentials obtained under canonical electrochemical conditions, rendering overpotential-rate comparisons meaningless between the two.
36. Tsuda, M.; Kasai, H., Imidazole ligand effect on O2 interaction with metalloporphyrins. *Surf. Sci.* **2007,** *601*, 5200–5206.
37. Ohta, T.; Nagaraju, P.; Liu, J.-G.; Ogura, T.; Naruta, Y., The secondary coordination sphere and axial ligand effects on oxygen reduction reaction by iron porphyrins: a DFT computational study. *J. Biol. Inorg. Chem.* **2016,** *21* (5), 745-755.

TOC:

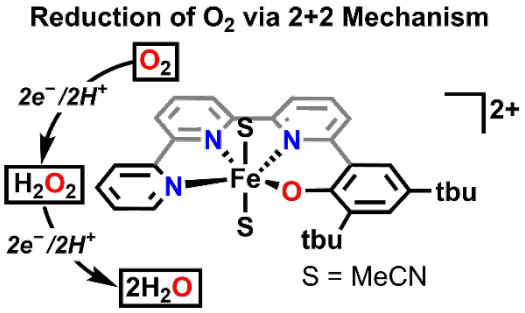

Synopsis:

A terpyridine-based non-heme iron complex containing a rigid monoanionic N_3O ligand framework catalytically reduces oxygen to water via a 2+2 mechanism. Electrochemical and mechanistic studies support the formation of H_2O_2 as a discrete intermediate before being reduced to two equivalents of H_2O during catalysis.